Spin density in frustrated magnets under mechanical stress: Mn-based antiperovskites

Pavel Lukashev and Renat F. Sabirianov
Department of Physics, University of Nebraska at Omaha, Nebraska 68188

Kirill Belashchenko
Department of Physics and Astronomy, University of Nebraska-Lincoln, Nebraska 68588

(Dated: September 9, 2009)

In this paper we present results of our calculations of the non-collinear spin density distribution in the systems with frustrated triangular magnetic structure (Mn-based antiperovskite compounds, Mn_3AN (A=Ga, Zn)) in the ground state and under external mechanical strain. We show that the spin density in the (111)-plane of the unit cell forms a "domain" structure around each atomic site but it has a more complex structure than the uniform distribution of the rigid spin model, i.e. Mn atoms in the (111)-plane form *non-uniform* "spin clouds", with the shape and size of these "domains" being function of strain. We show that both magnitude and direction of the spin density change under compressive and tensile strains, and the orientation of "spin domains" correlates with the reversal of the strain, i.e. switching compressive to tensile strain (and vice versa) results in "reversal" of the domains. We present analysis for the intra-atomic spin-exchange interaction and the way it affects the spin density distribution. In particular, we show that the spin density inside the atomic sphere in the system under mechanical stress depends on the degree of localization of electronic states.

PACS numbers:

I. 1. INTRODUCTION

In magnetic materials the local magnetic moments (LMM) are generally due to the d- and f- electrons. These electrons are localized, for example for 3d-metals the radius of d-orbitals is less than 1Å(*localized region (LR)*). On the other hand, s- and p-orbitals in 3d-metals are less localized or even delocalized (*delocalized region (DR)*). Thus, there are regions of high spin density (SD) in the LR near the nucleus and low SD further away in the DR. Despite the inhomogeneity of SD in magnetic materials, it is frequently described within the quasispin approximation [1], according to which the direction of the SD around each atom is taken constant within atomic sphere (AS) or polyhedron. This approach works better for the systems with strong spin-exchange coupling because the strong exchange between spins ensures that the SD direction stays almost uniform. Yet, for some systems it is essential to consider detailed distribution of magnetization axis as this may reveal additional important features of the magnetic configurations [2, 3] overlooked within the *rigid spin approximation* (RSA). In this paper we examine the SD distribution of the systems with frustrated magnetization, in particular Mn_3AN antiperovskites, using fully unconstrained SD functional without any assumption on the uniformity of SD around each atom.

Many interesting phenomena in magnetic materials are due to the interplay of magnetic and structural degrees of freedom because the SD is sensitive to mechanical deformations such as compression, in-plane biaxial strain, etc. In particular, such phenomena based on magneto-mechanical coupling have been reported for the Mn-based antiperovskites, - for example piezomagnetic effect [4], a giant magnetoresistance of more than 10% in pulsed magnetic fields [5], invar effect (or even negative thermal expansion) [6]. While the SD evolves under mechanical stress, the RSA assumes that its direction is changing uniformly inside of the AS. Yet, it is not obvious that in the excited states the spin moments in LR and DR rotate to the same angle. *We demonstrate in this paper that the spin directions in these two region may rotate in opposite directions.*

The ground state of Mn_3AN is shown in Fig. 1 (top panel). It forms an antiperovskite crystal structure with cubic space group *Pm3m*. The orientation of the LMMs of the Mn atoms forms a non-collinear, Γ^{5g} structure in the Bertaut's classification [7]. This is a structure with the spins on the (111)-plane with clockwise or counterclockwise spin configurations, such that the spin moments in the plane are canceling each other. This somewhat puzzling magnetic structure raises a natural question on how one treats the SD distribution in the system. In our previous work [4] we analyzed the piezomagnetic properties of Mn_3AN without presenting any details on the SD distribution, but rather we have discussed LMMs integrated over the atomic spheres.

The paper is organized as follows: in Section 2, we present results of our calculations of the magnetic properties of antiperovskite such as Mn_3ZnN under external stress; in Section 3, we present our results on the SD distribution in the (111)-plane of the unit cell, and we show that it has more complex structure than the one postulated in the RSA; in Section 4 we analyze the structure of the SD distribution in terms of the intra-atomic spin-exchange interaction; and finally, the last section is devoted to the conclusions.

We employ the projector augmented-wave (PAW) method originally proposed by P. Blöchl [8]. We use its implementation by G. Kresse and D. Joubert in the Vienna *ab* initio simulation package (VASP) code [9] within a Perdew-Burke-Ernzerhof (PBE) generalized gradient approximation [10] of the density functional theory (DFT). We use a $12 \times 12 \times 12$ k-point sampling and the Blöchl's tetrahedron integration method [11]. We set the plane-wave cut-off energy to 300 eV and we choose the convergence criteria for energy of 10^{-5} eV. Within this

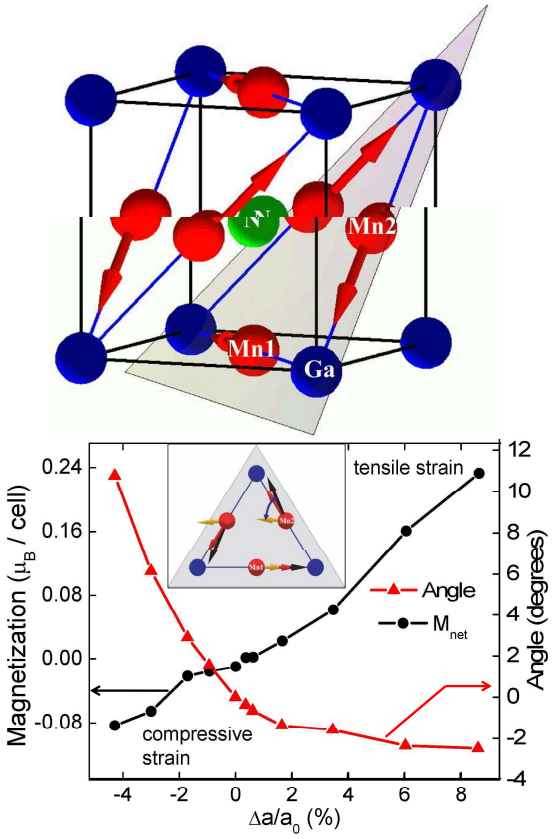

FIG. 1: (color online) Top panel: non-collinear Γ^{5g} structure, unit cell. Blue spheres - Ga atoms; red spheres - Mn atoms; green sphere - N atom. Arrows represent LMMs of Mn atoms. Bottom panel: the net magnetic moment per unit cell and the rotation angle of Mn2 LMMs as functions of biaxial strain (Δa/a (%)) in Mn_3ZnN. Inset on bottom panel: schematic view of the variation of Mn LMMs for Mn_3AN in (111)-plane as a function of strain. Yellow arrows - compressive strain, black arrows - tensile strain, red arrows - ground state.

framework we perform the non-collinear magnetic structure calculations, and we allow the LMMs to relax to the equilibrium configuration.

II. 2. MAGNETIC PROPERTIES OF MN-BASED ANTIPEROVSKITES UNDER STRESS

The equilibrium parameters for the Mn_3ZnN are as follows: 3.87Å for the lattice constant and 2.5 μ_B for the *LMM integrated over the volume of the space-filling AS*. The magnetic moment is extremely sensitive to the volume change. It steadily increases from 0.5 μ_B to 3.7 μ_B as the volume increases from the lattice parameter 3.5Å to 4.3Å. Application of the external strain results in induced magnetization. As one can see from the inset on the bottom panel of the Fig. 1 the magnetic moment of the Mn1 atom in the basal plane (formed by atoms of Mn and Ga) preserves its direction but its magnitude decreases/increses under compressive/tensile strain. LMMs of the Mn2 atoms in the Mn_2N plane change both their direction and magnitude, - they rotate towards the [110] direction when the compressive strain is applied in such a way that they become almost opposite to the LMM of Mn1 atom at large strains. The LMMs of Mn2 atoms become more aligned with each other (see Fig. 1, - inset on the bottom panel). When tensile strain is applied the LMMs of Mn2 atoms rotate in direction opposite to the one at the compressive strain and the Mn2 moments become more anti-aligned. The magnitude of the LMMs generally decreases with the compressive strain and increases with the tensile strain. Thus, Mn_3AN (A = Ga, Zn) antiperovskite acquires a net magnetization under biaxial strain as a result of the rotation of LMMs and change in their magnitude. The net magnetization is directed along the C_{2z} axis (this corresponds to a diagonal axis C_{2a} in the cubic cell). Fig. 1 (bottom panel) shows magnetization per cell (black line with solid circular data points) as a function of biaxial strain. The strain induced magnetization is about 0.07 μ_B per unit cell for the Mn_3ZnN at 3% of the compressive strain (for Mn_3GaN this value is substantially larger, in particular it is about 0.16 μ_B at 2% of the compressive strain). The piezomagnetic effect in Mn_3AN is *linear* and exhibits *magnetization reversal* with the applied strain, i.e. the direction of the magnetization along the C_{2z} axis reverses with the reversal of the applied strain. The rotation angle of the LMM of Mn2 atom under biaxial strain with respect to the Mn moment direction in the ground state as a function of strain is shown in Fig. 1 (bottom panel). The dependence is linear in the range of $\sim \pm 2\%$ of strain, and the LMMs rotate in opposite direction if the sign of the strain is reversed.

III. 3. SPIN DENSITY DISTRIBUTION

Fig. 2 shows the SD distribution in the (111)-plane of the unit cell for the non-collinear ground state Γ^{5g} structure of Mn_3AN. The overall structure of the SD in the (111)-plane resembles vortex with the center in the middle of the triangle formed by the Mn atoms. The orientation of the spin density in the center of the vortex is shown schematically on the inset of the Fig. 2. It reflects the anti-ferromagnetic nature of the inter-atomic exchange coupling of the nearest neighbor Mn atoms in the (111)-plane. Red arcs on the plot schematically show the AS within which the SD direction is assumed to be uniform by the quasispin approximation. As one can see from the plot, *this uniformity is only very approximate* as the magnetization axis direction clearly changes within the "quasispin domain". Particularly, in the LR (approximately inside r<0.7Å sphere) spin axis direction is more or less uniform. However, in the DR of low SD (approximately 0.7Å<r<1.4Å) the direction is changing substantially (by about 30 degrees).

Even more dramatic effect can be observed under strain, where regions of SD inside AS rotate in opposite directions. To better visualize the non-uniformity of SD we plot the vector product of the magnetizations in the ground state and under strain

(**m**(equilibrium)×**m**(strain)) in the (111)-plane (see Figure 3). The out of plane arrows (green) show counterclockwise rotations, while into the plane arrows (blue) show clockwise rotations of SD under strain. One can clearly visualize from Figure 3 the appearance of domains with different direction of SD rotation. Particularly, there are relatively large domains in DR which rotate opposite to the domains in LR. Therefore, the SD distribution in the (111)-plane is more complex than the ideal picture of the uniform SD around each atom assumed by the RSA. To understand this "beyond RSA" pattern we analyze the intra-atomic spin-exchange interaction and the way it affects the SD around each atom.

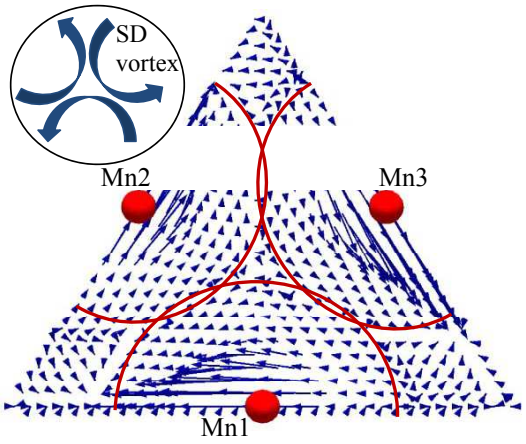

FIG. 2: (color online) Spin density distribution in (111)-plane for the non-collinear Γ^{5g} structure of Mn_3AN, unit cell. Red spheres represent Mn atoms. Red arcs schematically highlight SD distribution "domains" around each Mn atom. Blue arrows represent SD direction. Inset schematically shows the orientation of the spin density in the center of the vortex.

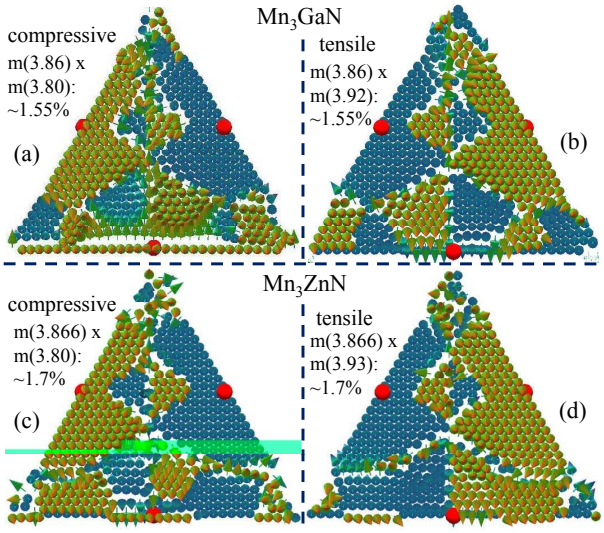

FIG. 3: (color online) Vector product of the local SD in the ground state and under strain in the (111)-plane: Mn_3GaN (a, b) and Mn_3ZnN (c, d): red spheres represent Mn atoms; green (light) domains represent out-of-plane vector product direction; blue (dark) domains represent into-the-plane vector product direction.

$$E_{ex.}(\theta) = -\int_{x2}^{x3} dxdx' \underbrace{J(x,x')S_xS_{x'}cos(\theta_x - \theta_{x'})}_{H(x,x')} \Rightarrow$$

$$E_{ex.} \approx const + \frac{1}{2}\int_{x2}^{x3} dxdx' J(x,x')s_xs_{x'}e^{-\frac{x+x'}{\lambda}}(\delta\theta)^2$$

$$= const + \frac{1}{2}\int_{x2}^{x3} dxJ(x)s_x^2 e^{-\frac{x}{\lambda/2}}(\delta\theta)^2 \quad (1)$$

where $J(x,x')$ is the exchange parameter; S_x and $S_{x'}$ are spin vectors at x and x'; x and x' are "spin positions" along Mn2↔Mn3 line; $x2$ and $x3$ are coordinates of the Mn2 and Mn3 atoms; θ_x and $\theta_{x'}$ are angles between spin at x and x' and z-axis. Besides, here we used the exponential behavior of the magnitude of the spin vector (see Fig. 4, bottom panel), and δ-function-like behavior of $J(x,x')$, i.e.

$$S_xS_{x'} = s_xs_{x'}e^{-\frac{x+x'}{\lambda}} \quad (2)$$

$$J(x,x')s_{x'}dx' = J(x)s_x \quad (3)$$

We also assume that x and x' are very close to each other, therefore $x + x' \approx 2x$.

To find the expression for the $\theta(x)$ which fits the SD distribution shown on Fig. 4 (top panel) we have to minimize Eq.1 w.r.t. x, i.e. we have to set the functional derivative of Eq.1 equal to zero. This results in the following differential equation with the boundary conditions:

IV. 4. DISCUSSION

To simplify our analysis we consider SD along the line between Mn2 and Mn3 atoms, i.e. we reduce 3-dimensional problem to 1-dimensional. Fig. 4 (top panel) shows the ground state SD distribution for the Mn_3GaN along the lines connecting Mn atoms in the (111)-plane of the unit cell. *The angle, θ between the SD direction (blue arrows on the plot) and the z-axis (normal to the line between Mn2 and Mn3 atoms) does not show the uniformity inside AS around each Mn atom assumed in the RSA*. Fig. 4 (bottom panel) shows the magnitude of the SD, $|\mathbf{m}|$ as a function of distance between Mn2 and Mn3 atoms. Like θ, the $|\mathbf{m}|$ also shows distinct non-uniform behavior. Qualitatively these features of SD distribution can be interpreted in terms of the spin-exchange interactions. For *continuous* SD distribution the spin-exchange contribution to the interaction energy between Mn2 and Mn3 atoms can be written in terms of the spin (Heisenberg) Hamiltonian, $H(x,x')$ [13] as follows:

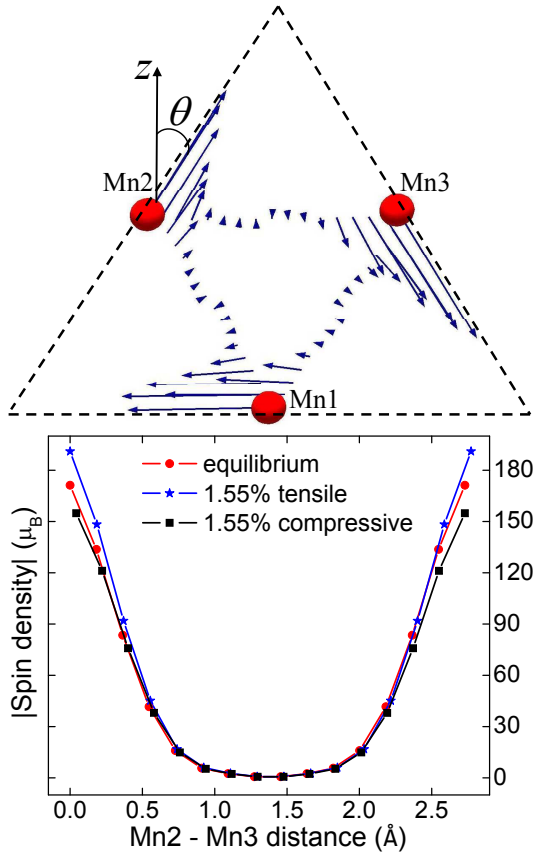

FIG. 4: (color online) Magnetization distribution between Mn atoms in (111)-plane for the non-collinear Γ^{5g} structure of Mn_3GaN (top panel); |Spin density| as a function of distance between Mn2 and Mn3 (bottom panel) for ground state (red), 1.55% tensile strain (blue), and 1.55% compressive strain (black).

$$J(x)\cdot\ddot{\theta}(x)+\dot{\theta}(x)\cdot\dot{J}(x)=0;$$
$$\theta(x2)=30^0;\ \ \theta(x3)=-30^0 \qquad (4)$$

from which

$$e^{-\frac{x}{\lambda/2}}\cdot\frac{d^2}{d^2x}\theta(x)+\frac{d}{dx}\theta(x)\cdot\frac{d}{dx}e^{-\frac{x}{\lambda/2}}=0;$$
$$\theta(x2)=30^0;\ \ \theta(x3)=-30^0 \qquad (5)$$

We solve this equation separately for LR and DR by choosing the value for λ which corresponds to the best fit for the distribution of θ as a function of distance between Mn2 and Mn3 atoms. Results of the solutions for the ground state and strained Mn_3GaN are summarized on Fig. 5 (top panel) and Table I.

Fig. 5 (top panel) shows the change in θ for Mn_3GaN along the half-distance of the line connecting Mn2 and Mn3 atoms for the ground state, tensile strain (∼1.55%), and compressive strain (∼1.55%) (for the other half of the Mn2-Mn3 distance we just have to change the sign of θ). As one can see the angle θ under tensile strain for the SD distribution in the LR is lower than the θ for the

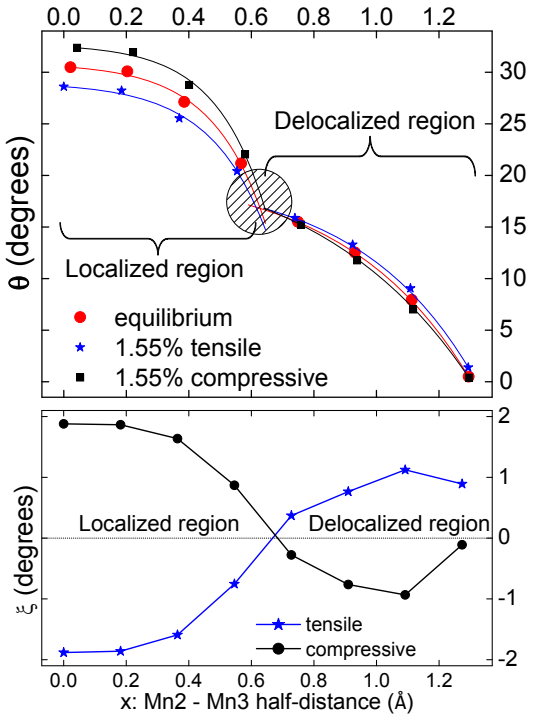

FIG. 5: (color online) Top panel: θ as a function of half-distance between Mn2 and Mn3 atoms for ground state (red spheres), 1.55% tensile strain (blue stars), and 1.55% compressive strain (black squares). Bottom panel: ξ as a function of half-distance between Mn2 and Mn3 atoms.

$J(x)$ and θ	Equilibrium	1.55% tens.	1.55% compr.
$J(x)$(LR)	$e^{-x/0.17}$	$e^{-x/0.18}$	$e^{-x/0.16}$
$J(x)$(DR)	$e^{-x/0.40}$	$e^{-x/0.37}$	$e^{-x/0.50}$
θ(LR)	31-0.35·$e^{5.9\cdot x}$	29-0.40·$e^{5.6\cdot x}$	33-0.29·$e^{6.3\cdot x}$
θ(DR)	21-0.79·$e^{2.5\cdot x}$	20-0.57·$e^{2.7\cdot x}$	23-1.69·$e^{2\cdot x}$

TABLE I: $J(x)$ and $\theta(x)$ for the Mn_3GaN in the ground state and under strain for regions of localized (LR) and delocalized (DR) electronic states.

ground state in the same region. This is consistent with the general description of the piezomagnetic effect presented above, - see for example the inset on the bottom panel of the Fig. 1. Yet, in the DR the ground state θ becomes smaller, right up to the point when θ changes the sign. Under compressive strain the θ is larger for the SD distribution in the LR than the θ for the ground state in the same region (again, consistent with the description of the piezomagnetism presented above). Closer to the DR the difference in angles for the system under compressive strain and for the system in equilibrium decreases and finally changes its sign, after which the θ for the ground state becomes larger than the θ for the compressed system. But for both signs of the strain (tensile and compressive) the magnitude of the difference in the θ for the strained and equilibrium states ($\xi \stackrel{\text{def}}{=} \theta$*(under strain) - θ(equilibrium)*$|_{\theta\geq 0 or \theta\leq 0}$*) is larger in the LR compared to the DR (see Fig. 5 (bottom panel)). This ξ sign

changing mechanism is obviously in agreement with the SD distribution picture shown on the Fig. 3 (see for example (a) and (b), - both show the reversal of the sign of the $\mathbf{m}$(equil.)$\times\mathbf{m}$(strain) at the border of the LR/DR domains. *These "additional spin domains" in DR cannot be revealed within the RSA framework.* The sign of ξ is changing because the strain affects the overlap of the wave functions (spin-exchange interaction). For example, when tensile strain is applied the distance between Mn2 and Mn3 atoms increases which results in increased localization of the electronic states in the LR (in $J(x)$ λ increases from 0.17 to 0.18, - see Table I). At the same time, $J(x)$ of delocalized states in the DR becomes weaker (λ decreases from 0.40 to 0.37). This decrease in $J(x)$ in the DR results in reversal of the ξ sign, which in its turn leads to appearance of the additional "domains" on Fig. 3. On the other hand, when compressive strain is applied, the states in the LR become less localized (λ decreases from 0.17 to 0.16) while the $J(x)$ in DR becomes stronger (λ increases from 0.40 to 0.50). This $J(x)$ increase in DR under compressive strain also results in reversal of the ξ sign (as in the case of the tensile strain the spins in LR and DR turn in different directions). All the above arguments based on our model present general idea of the mechanisms responsible for the "beyond RSA" picture.

V. 6. CONCLUSION

We have presented results of our calculations on the spin density distribution of the Mn_3AN in the ground state and under external bi-axial strain. In both cases the spin density demonstrates non-uniform features such as appearance of additional spin domains in the (111)-plane not revealed within the quasispin approximation. The orientation of the spin density depends on the direction of the strain. We have presented explanation of the non-uniform distribution of the spin density in terms of the intra-atomic spin-exchange interaction. In particular we have shown that the spin density distribution depends on the degree of localization of the electronic orbitals, i.e. strongly and weakly localized orbitals within the same atomic sphere rotate in different directions under external strain.

VI. ACKNOWLEDGEMENT

This work was supported by the Nebraska Research Initiative, the National Science Foundation and the Nanoelectronics Research Initiative through the Materials Research Science and Engineering Center at the University of Nebraska.

[1] S. H. Liu "Quasispin model of itinerant magnetism", Phys. Rev. B. 13, 3962, 1976
[2] Adrian Taga, Lars Nordström, Peter James, Börje Johansson & Olle Eriksson, Nature **406**, 280 (2000).
[3] D. Hobbs and J. Hafner, J. Phys.: Condens. Matter **12** (2000) 7025-7040.
[4] P. Lukashev, R. Sabirianov, and K. Belashchenko, Phys. Rev. B **78**, 184414 (2008).
[5] K. Kamishima, T. Goto, H. Nakagawa, N. Miura, M. Ohashi, and N. Mori, T. Sasaki and T. Kanomata, Phys. Rev. B **63**, 024426 (2000).
[6] K. Takenaka, and H. Takagi, Applied Physics Letters **87**, 261902 (2005).
[7] E.F. Bertaut, D. Fruchart, J.P. Bouchaud and R. Fruchart, Solid State Commun. **6**, 251 (1968).
[8] P. Blöchl, Phys. Rev. B **50**, (1994) 17953.
[9] G. Kresse and D. Joubert, Phys. Rev. B **59**, (1999) 1758.
[10] J.P. Perdew, K. Burke, and M. Ernzerhof, Phys. Rev. Lett. **77**, 3865 (1996).
[11] P.E. Blöchl , O. Jepsen, O.K. Andersen, Phys. Rev. B **49**, 16223 (1994).
[12] H. Liu, S.N. Zhu, Y.Y. Zhu, Y.F. Chen, and N.B. Ming, X. Zhang, Appl. Phys. Lett. **86**, 102904 (2005).
[13] N.W. Ashcroft and N.D. Mermin, Solid State Physics, (Holt, Rinehart, and Winston, New York, 1976).